The Astrophysical Journal, 882:97 (5pp), 2019 September 10 https://doi.org/10.3847/1538-4357/ab35e1

Hydrogen Emission in Type II White-light Solar Flares

Ondřej Procházka, Aaron Reid, and Mihalis Mathioudakis
Astrophysics Research Centre, Queen's University Belfast, Northern Ireland, UK; oprochazka01@qub.ac.uk
Received 2019 March 8; revised 2019 June 27; accepted 2019 July 24; published 2019 September 6

Abstract

Type II white-light flares (WLFs) have weak Balmer line emission and no Balmer jump. We carried out a set of radiative hydrodynamic simulations to understand how the hydrogen radiative losses vary with the electron-beam parameters and more specifically with the low-energy cutoff. Our results have revealed that for low-energy beams, the excess flare Lyman emission diminishes with increasing low-energy cutoff as the energy deposited into the top chromosphere is low compared to the energy deposited into the deeper layers. Some Balmer excess emission is always present and is driven primarily by direct heating from the beam with a minor contribution from Lyman continuum backwarming. The absence of Lyman excess emission in electron-beam driven models with high low-energy cutoff is a prominent spectral signature of type II WLFs.

Key words: methods: numerical – radiative transfer – Sun: chromosphere – Sun: flares

1. Introduction

White-light flares (WLFs) have attracted considerable attention since the Carrington event in 1859 when brightenings lasting for several minutes were observed in the solar photosphere (Carrington 1859). Early spectroscopic observations have shown that hydrogen emission dominates the excess spectrum of WLFs with the Balmer lines, in particular increasing considerably above the quiescent level (Švestka 1966; Machado & Rust 1974). Early observations used the area of the emitting chromosphere as seen in Hα together with the intensity of the emission to classify flares. The Hα line is still routinely used to image the upper layer of the chromosphere that is greatly affected during the flare event. The first multichannel flare observations covering the Lyα that showed excess emission during a solar flare were obtained with the Laboratoire de Physique Stellarie et Planétaire (LPSP) instrument (Bonnet et al. 1978) on board the *OSO-8* satellite (Maran & Thomas 1975; Lemaire et al. 1984). The continuous monitoring of solar irradiance in Lyα commenced in 2006 with the EUV Sensor (Viereck et al. 2007) on board the *Geostationary Environmental Operational Satellite* (*GOES*). The Extreme-ultraviolet Variability Experiment (EVE; Woods et al. 2012) on board the *Solar Dynamics Observatory* allowed the regular acquisition of flare spectra covering the Lyman lines and continuum. The analysis of solar flares showed a rapid increase in Lyα during the impulsive phase (Milligan & Chamberlin 2016) consistent with the Hα line behavior. Machado et al. (2018) used the EVE to study the departure coefficients and the color temperature of six X-class flares. They found a rapid increase in the Lyman continuum during the impulsive phase originating in a thin layer where the electron density exceeded 10^{13} cm^{-3}.

The existence of two spectrally distinct types of WLFs was first reported by Machado et al. (1986). Their conclusion was based on the analysis of flaring spectra in the near-UV and visible range (Hiei 1982; Neidig 1983; Boyer et al. 1985) where they identified rare events with extraordinarily weak and narrow Balmer lines and without a Balmer jump. They named such events type II WLFs but were not able to explain theoretically the difference between these events and flares with strong and broad Balmer lines (type I WLFs). Ding et al. (1999) proposed a scenario different from the standard flare model that incorporated an energy release in the lower layers of the solar atmosphere to explain the suppressed hydrogen emission in the type II WLFs. Their interpretation included an initial decline in the WL continuum just before the flare onset and was also elaborated by Litvinenko (1999) and Chen et al. (2001). Allred et al. (2005) compared the atmospheric response due to electron-beam heating of 10^{10} and 10^{11} erg cm^{-2} s^{-1} and found that the initial decline in continuum can be caused by nonthermal hydrogen ionization. They found that for the lower beam flux the decline lasts longer and therefore is more likely to be detected during the observations. Matthews et al. (2003) carried out a large study of 59 WLFs observed with the Yohkoh spacecraft. However, the lack of spectral information did not allow them to identify with certainty the atmospheric height where the observed emission originated and were unable to distinguish between type I and type II WLFs. Despite these efforts, the exact definition of type II WLFs remains unclear. While it is largely accepted that these events are characterized by suppressed Balmer line emission, some of their other features are questionable due to the lack of sufficient observational diagnostics. For example, the time lag between the WL emission, hard X-ray (HXR) emission, and microwave emission is thought to be a feature of the type II WLFs (Fang & Ding 1995). However, Procházka et al. (2017, 2018) presented a multi-instrument study of a type II WLF and found no temporal mismatch between WL, HXR, and γ-ray emissions. Their work showed that type II WLFs are consistent with the standard flare model, and their spectral signatures can be explained with low-energy particle beams with a high value for the low-energy cutoff. Such beams are able to leave the upper chromosphere relatively undisturbed and deposit their energy into the deeper layers of the atmosphere.

In this paper we use the radiative hydrodynamic code RADYN to analyze the hydrogen emission in flares that are driven by electron beams with parameters that are representative of type I and type II WLFs. We use the models of Procházka et al. (2018) that identified the best set of

electron-beam parameters that can recreate the observational signatures of the X1-class flare on 2014 June 14. The selected electron-beam-driven models are then used to evaluate the radiative losses in both Lyman and Balmer transitions.

2. Flare Modeling

The RADYN code (Carlsson & Stein 1992, 1995, 1997; Allred et al. 2015) is a one-dimensional radiative hydrodynamic code that can be used to study the interaction of particle beams with the solar atmosphere. It uses the Fokker–Planck formalism (McTiernan & Petrosian 1990), which takes into account the beam energy losses due to Coulomb collisions and pitch-angle diffusion when incorporating relativistic effects. RADYN includes a six-level hydrogen atom, a nine-level helium atom, and a six-level calcium atom. A return current has also been included in the simulations. We generated a set of models that simulates the conditions in the solar atmosphere during weak to intense WLFs. The beam fluxes used had values of 3×10^9, 1×10^{10}, and 3×10^{10} erg cm^{-2} s^{-1}, while the low-energy cutoff E_C covered the parameter space where flare values are usually found (20–120 keV; Warmuth & Mann 2016). The spectral index δ was equal to 3 for all models. The beams were applied continuously and the outputs were analyzed at $t = 20$ s. This value is consistent with the X-ray analysis of the best observed type II WLF to date (Procházka et al. 2018). The initial atmosphere used in this work has the transition region placed at a height of 1200 km above the photospheric floor and has a coronal temperature of 3 MK at 10 Mm (QS.SL.HT loop described in Allred et al. 2015). The beams were injected at the top of a half-loop with a Gaussian distribution with an HWHM of 23°.5. Line synthesis was carried out using the RH code (Uitenbroek 2001) incorporating partial redistribution that is particularly important for resonance line profiles. We used the 20-level hydrogen atom and the 6-level calcium atom to produce synthetic spectra for the Lyman and Balmer line and continuum diagnostics. A VOIGT profile was used for Ca II K line, Lyman γ the higher-order Lyman lines. The Ca II H and Lyα and β profiles were modeled in PRD. The Balmer lines had profiles of type VOIGT_VCS_STARK, which incorporates the unified Stark effect theory (Kowalski et al. 2017). The spectra were synthesized by setting a minimal spectral resolution of 0.05 nm.

3. Results

Figure 1 shows the radiative losses and energy input per unit mass across the atmosphere due to the most important hydrogen transitions in models with the beam flux equal to 3×10^9 erg cm^{-2} s^{-1}. The figure shows that beams with a low E_C (20 keV) disrupt the top chromosphere, shift the transition region to heights of up to 1500 km, and produce emission in the Lyman continuum and Lyα. The figures also show a peak of absorption in the Lyman continuum at the same height where we can see the maximum of radiative losses in the Balmer and the higher-order continua. This means that the Lyman continuum irradiated downward contributes to hydrogen ionization in the deeper layers. The radiative losses for E_C greater than 40 keV do not show any such Lyman emission, but they still show the emission in the higher-order continua that are clearly driven by the particle-beam precipitation.

Table 1 shows the gross radiative losses in the atmosphere due to the free–bound Lyman and Balmer transitions (LyC and BaC, respectively) and the bound–bound Lyα and Hα transitions, respectively. The radiative losses were integrated only over the chromosphere and the temperature minimum region—between the height of 300 km above the photospheric floor and the height where the temperature begins to exceed 10^5 K. These numbers do not include any possible reabsorption outside these atmospheric heights; therefore, they do not quantify the radiative output of the atmosphere as seen by an observer. The table shows that there is an overall stronger emission for particle beams with higher flux with the LyC showing the greatest variation. In models with $E_C = 20$ keV the LyC losses reach values of 10^{19}–10^{20} erg cm s^{-1} g^{-1}; however, models with high E_C show that the LyC remains at the quiet level ($\sim 10^{16}$ erg cm s^{-1} g^{-1}). The situation is the same for the Lyα, where the quiet level reaches $\sim 10^{17}$ erg cm s^{-1} g^{-1}. The radiative losses listed in Table 1 show that when the beam flux is increased, the maximum radiative losses in the studied lines and continua occur at higher values of E_C. With increasing E_C it is the LyC that reaches the peak of the radiative losses first and then the Balmer continuum. This is due to the greater penetration depth of the beams with higher E_C and the fact that the LyC originates higher in the atmosphere than the BaC.

Figure 2 shows the RH synthetic spectra for the electron-beam-driven models with a flux of 3×10^9 erg cm^{-2} s^{-1} in the wavelength range that covers the higher-order Lyman lines and LyC, the Lyα, the higher-order Balmer lines, and BaC. The figure shows a qualitative difference between the Lyman and Balmer emission. The Balmer emission, which is especially well illustrated on the BaC level, gradually decreases with increasing E_C; the LyC is only detected for low values of E_C. Figure 3 shows that for beam fluxes less than 1×10^{10} erg cm^{-2} s^{-1} we can find E_C within the modeled range, for which the excess radiative losses in the LyC are almost zero. In the spectrum (Figure 2) this is manifested as no excess emission in the LyC and no rise of the Lyα peak emission (Figure 4).

4. Discussion and Concluding Remarks

We have used radiative hydrodynamic models to study the atmospheric response to electron-beam-driven heating. Our analysis has shown that for sufficiently low electron-beam fluxes and sufficiently high E_C the flaring atmosphere does not produce any significant excess emission in the Lyman lines and continuum. These beam parameters still produce excess emission in the higher-order hydrogen transitions, such as the Balmer or Paschen continua. This is due to the different atmospheric layers where the emission originates. The LyC is produced at the top of the chromosphere, which during flares is disturbed by the low-energy particles, whereas the higher-order continua are produced deeper in the atmosphere, and their excess emissions therefore appear in all our models (Figure 1). The particle beams with the high E_C do not contain the low-energy particles that would be stopped at the top of the chromosphere; hence, they do not yield excess flare emission in the LyC. The lack of a response in the LyC can be considered as an intriguing result as the type II flare that our models are based on has a *GOES* X1.0 classification and hence a strong X-ray emission.

Flares with no Lyman emission have not been reported in the literature. This may be due to the lack of suitable observational data and the sparsity of flare beams with sufficiently high E_C (Fletcher et al. 2007). Milligan et al. (2014) published an

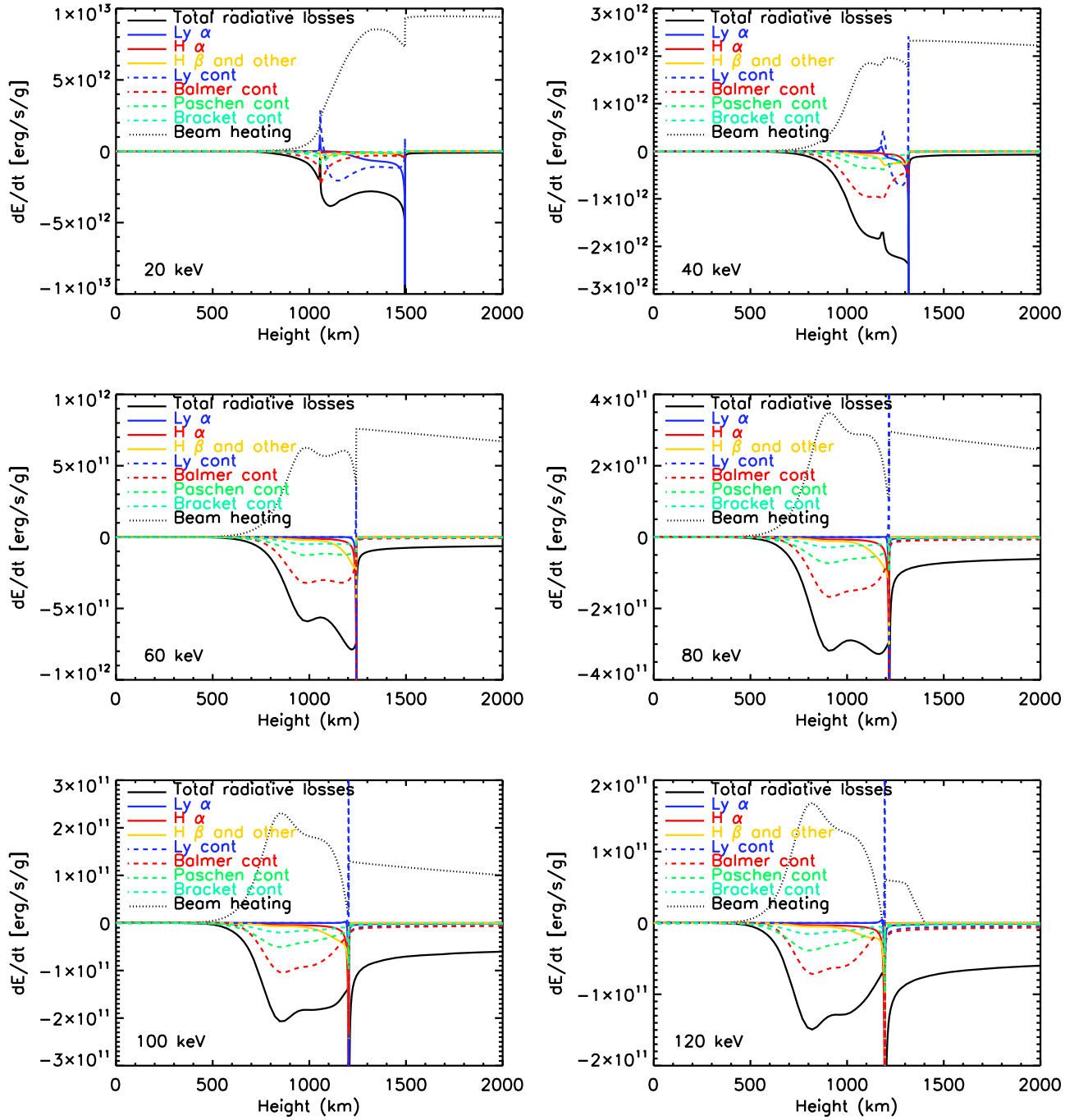

Figure 1. Radiative losses during the flare electron-beam precipitation for E_C in the range of 20–120 keV. The beam flux is equal to 3×10^9 erg cm^{-2} s^{-1}. A positive (negative) $\frac{dE}{dt}$ corresponds to absorption (emission). The profiles are taken 20 s into the simulations.

extensive multi-instrument analysis of a type I X-class solar flare and found that the Lyα dominated the measured radiative losses. Their upper estimates of the E_C and the beam flux were in ranges of 21.8–25.9 keV and 2.7×10^{10}–4.7×10^{11} erg cm^{-2} s^{-1}, respectively, and therefore were more energetic than those studied in our work. We speculate that they found the Lyα to dominate the radiative losses because its core is formed at the top chromosphere and transition region (Vernazza et al. 1981), and therefore is not subjected to significant reabsorption by the overlying layers of the atmosphere. On the other hand, the continua are formed in the deeper layers of the atmosphere, and even if a significant portion of energy is emitted in these transitions, only a fraction of the energy can be detected due to reabsorption. Indeed, they estimate that the detected energy in the EUV H I, He I, He II continua; the He II (30.4 nm) and Lyα lines; the UV continua at 160 and 170 nm; the WL continua at 450.4, 555.0, and 668.4 nm; and the Ca II H line (396.8 nm) accounted for not more than 15% of the total energy delivered to the atmosphere by the electron beams. The Spectral Investigation of the Coronal Environment (Fludra et al. 2013) instrument on board the Solar Orbiter, which is due to be launched in 2020, will record spectra in the wavelength ranges 70.4–79.0 nm and

Table 1
Atmospheric Heating and Radiative Losses Due to the Hydrogen Transitions in Electron-beam-driven Models

	E_C (keV)	Beam Heating (erg cm s^{-1} g^{-1})	Losses in LyC (erg cm s^{-1} g^{-1})	Losses in BaC (erg cm s^{-1} g^{-1})	Losses in Lyα (erg cm s^{-1} g^{-1})	Losses in Hα (erg cm s^{-1} g^{-1})
		0	2.13e+16	1.27e+16	2.98e+17	1.41e+17
$F = 3 \times 10^9$ erg cm^{-2} s^{-1}	20	3.15e+20	5.63e+19	3.39e+19	2.29e+19	5.09e+18
	40	6.52e+19	5.99e+18	2.94e+19	3.08e+18	2.61e+18
	60	2.39e+19	1.47e+16	1.21e+19	4.29e+17	1.09e+18
	80	1.35e+19	1.79e+16	6.40e+18	3.33e+17	7.03e+17
	100	8.97e+18	1.84e+16	3.97e+18	3.08e+17	5.27e+17
	120	6.54e+18	1.99e+16	2.68e+18	3.03e+17	4.27e+17
$F = 1 \times 10^{10}$ erg cm^{-2} s^{-1}	20	1.03e+21	1.04e+20	6.67e+19	4.26e+19	5.97e+18
	40	4.42e+20	8.58e+19	7.20e+19	2.49e+19	5.73e+18
	60	1.65e+20	4.01e+19	5.77e+19	1.34e+19	4.71e+18
	80	7.98e+19	1.93e+19	4.01e+19	6.66e+18	3.54e+18
	100	4.52e+19	3.67e+18	2.91e+19	2.58e+18	2.45e+18
	120	2.92e+19	4.98e+16	1.94e+19	7.12e+17	1.59e+18
$F = 3 \times 10^{10}$ erg cm^{-2} s^{-1}	20	1.35e+21	1.35e+20	9.20e+19	2.89e+19	4.47e+18
	40	1.59e+21	1.58e+20	1.34e+20	4.59e+19	6.98e+18
	60	8.02e+20	1.21e+20	1.38e+20	4.00e+19	7.09e+18
	80	4.19e+20	8.36e+19	1.15e+20	3.52e+19	6.81e+18
	100	2.42e+20	6.80e+19	8.89e+19	2.78e+19	6.14e+18
	120	1.52e+20	5.35e+19	7.14e+19	2.08e+19	5.47e+18

Note. The radiative losses and the beam heating, as shown in Figure 1, were integrated over the temperature minimum region and chromosphere. The first row shows the radiative losses for the quiet atmosphere.

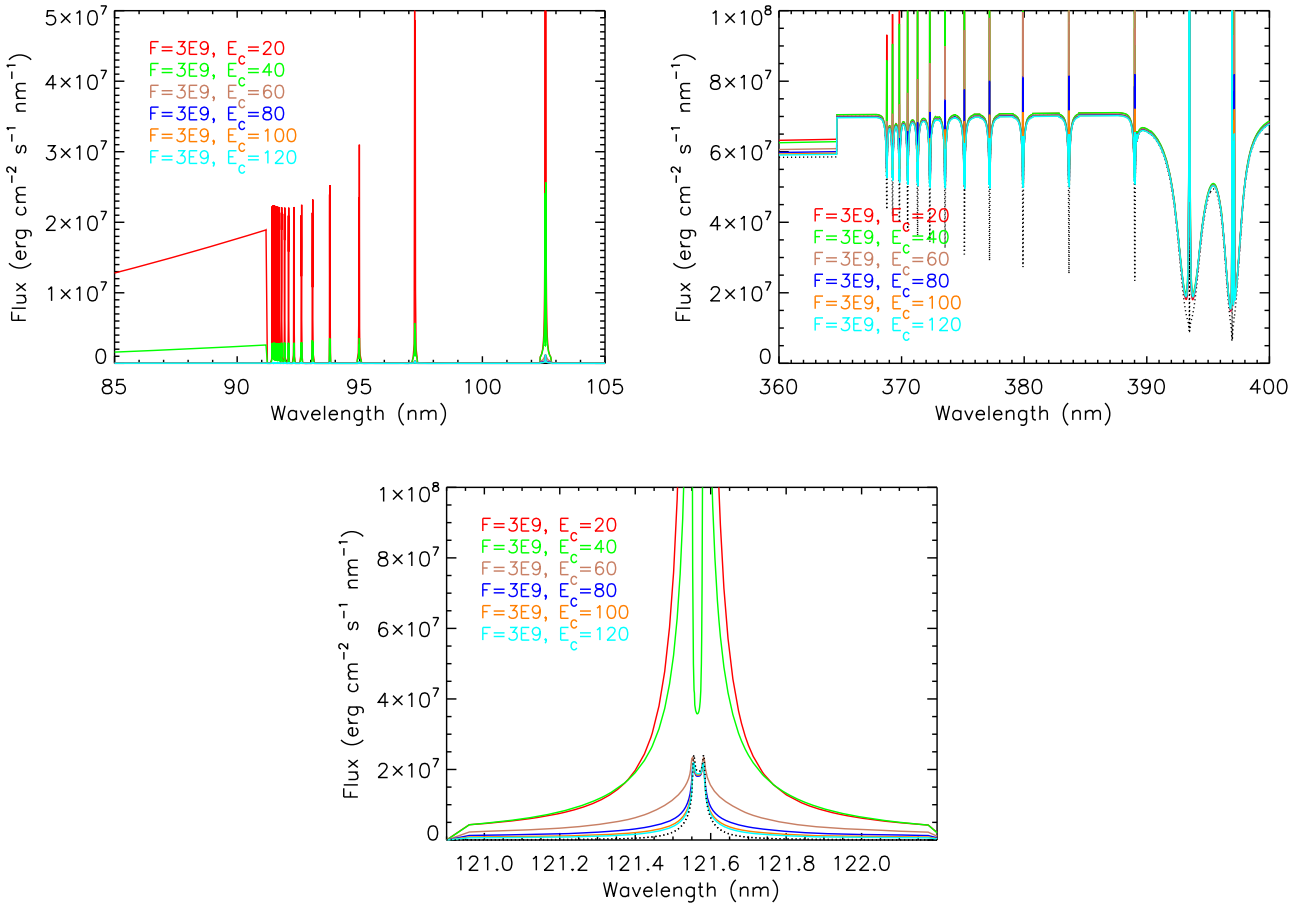

Figure 2. RH synthetic spectra from the electron-beam-driven models with a beam flux of 3×10^9 erg cm^{-2} s^{-1}. The dotted line marks the quiescent profiles.

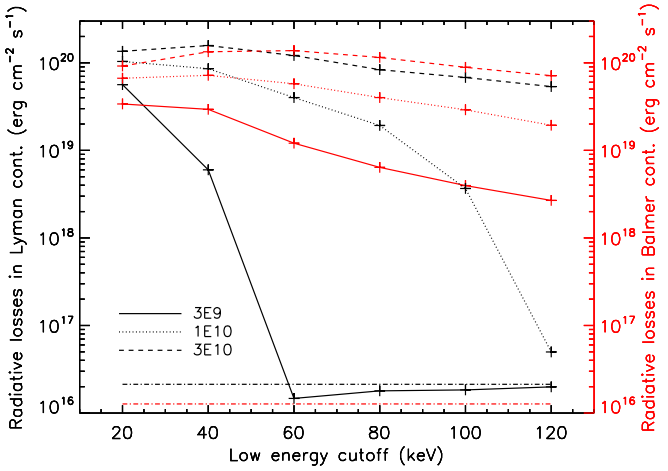

Figure 3. Gross radiative losses between the photosphere and the transition region due to the Lyman and Balmer free–bound transitions as a function of E_C. The legend distinguishes between the beam flux. The dotted–dashed lines mark the level of the radiative losses with no beam applied.

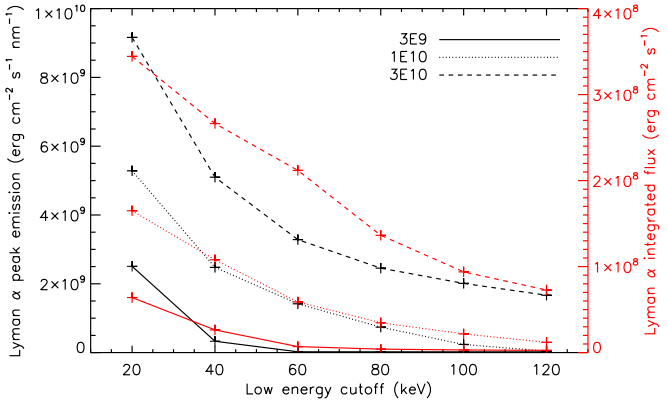

Figure 4. Spectral characteristics of Lyα line for a range of E_C and beam flux equal to 3×10^{10} erg cm^{-2} s^{-1}. The line flux was integrated over 1.2 nm with the line core being in the center of the integrated wavelength region.

97.3–104.9 nm. These spectral ranges cover the higher Lyman lines and continuum as well as lines from several ionized species formed at temperatures from 10,000 to 10 million K.

Particle beams with an E_C greater than 100 keV were directly observed only once by Warmuth et al. (2009), but they were also found to be consistent with the spectral features of type II WLFs (Procházka et al. 2018). Their work confirms that these beams produce a weaker excess Balmer emission than the low E_C particle beams consistent with the definition of the type II WLFs. From an observational point of view it is easier to detect the flare excess in the Lyman lines and continuum due to the absence of a strong background spectrum. Our work shows that the absence of an excess emission in the LyC and no increase of the Lyα peak emission are the best indicators of the type II WLFs and for the first time reveals their qualitative difference with the type I events. The definition of type I and type II WLFs has been traditionally based on the observational signatures that emanate from the hydrogen Balmer lines and continuum (Machado et al. 1986). The *IRIS* mission has acquired a large number of flare data sets that provide a wealth of upper chromospheric and transition region diagnostics that may also be used to discriminate between these two types of flare events.

The research leading to these results has received funding from the European Community's Seventh Framework Programme (FP7/2007–2013) under grant agreement No. 606862 (F-CHROMA). We would like to thank Joel Allred, Mats Carlsson, Adam Kowalski, and Han Uitenbroek for the development of the numerical codes used in this study.

ORCID iDs

Ondřej Procházka https://orcid.org/0000-0003-4215-5062
Aaron Reid https://orcid.org/0000-0002-7695-4834
Mihalis Mathioudakis https://orcid.org/0000-0002-7725-6296

References

Allred, J. C., Hawley, S. L., Abbett, W. P., & Carlsson, M. 2005, ApJ, 630, 573
Allred, J. C., Kowalski, A. F., & Carlsson, M. 2015, ApJ, 809, 104
Bonnet, R. M., Lemaire, P., Vial, J. C., et al. 1978, ApJ, 221, 1032
Boyer, R., Sotirovsky, P., Machado, M. E., & Rust, D. M. 1985, SoPh, 98, 255
Carlsson, M., & Stein, R. F. 1992, ApJL, 397, L59
Carlsson, M., & Stein, R. F. 1995, ApJL, 440, L29
Carlsson, M., & Stein, R. F. 1997, ApJ, 481, 500
Carrington, R. C. 1859, MNRAS, 20, 13
Chen, P.-F., Fang, C., & Ding, M.-D. D. 2001, ChJAA, 1, 176
Ding, M. D., Fang, C., & Yun, H. S. 1999, ApJ, 512, 454
Fang, C., & Ding, M. D. 1995, A&AS, 110, 99
Fletcher, L., Hannah, I. G., Hudson, H. S., & Metcalf, T. R. 2007, in ASP Conf. Ser. 368, The Physics of Chromospheric Plasmas, ed. P. Heinzel, I. Dorotovič, & R. J. Rutten (San Francisco, CA: ASP)
Fludra, A., Griffin, D., Caldwell, M., et al. 2013, Proc. SPIE, 8862, 88620F
Hiei, E. 1982, SoPh, 80, 113
Kowalski, A. F., Allred, J. C., Uitenbroek, H., et al. 2017, ApJ, 837, 125
Lemaire, P., Choucq-Bruston, M., & Vial, J.-C. 1984, SoPh, 90, 63
Litvinenko, Y. E. 1999, ApJ, 515, 435
Machado, M. E., Avrett, E. H., Falciani, R., et al. 1986, in The Lower Atmosphere of Solar Flares, ed. D. F. Neidig, 483
Machado, M. E., Milligan, R. O., & Simões, P. J. A. 2018, ApJ, 869, 63
Machado, M. E., & Rust, D. M. 1974, SoPh, 38, 499
Maran, S. P., & Thomas, R. J. 1975, S&T, 49, 355
Matthews, S. A., van Driel-Gesztelyi, L., Hudson, H. S., & Nitta, N. V. 2003, A&A, 409, 1107
McTiernan, J. M., & Petrosian, V. 1990, ApJ, 359, 524
Milligan, R. O., & Chamberlin, P. C. 2016, A&A, 587, A123
Milligan, R. O., Kerr, G. S., Dennis, B. R., et al. 2014, ApJ, 793, 70
Neidig, D. F. 1983, SoPh, 85, 285
Procházka, O., Milligan, R. O., Allred, J. C., et al. 2017, ApJ, 837, 46
Procházka, O., Reid, A., Milligan, R. O., et al. 2018, ApJ, 862, 76
Švestka, Z. 1966, SSRv, 5, 388
Uitenbroek, H. 2001, ApJ, 557, 389
Vernazza, J. E., Avrett, E. H., & Loeser, R. 1981, ApJS, 45, 635
Viereck, R., Hanser, F., Wise, J., et al. 2007, Proc. SPIE, 6689, 66890K
Warmuth, A., Holman, G. D., Dennis, B. R., et al. 2009, ApJ, 699, 917
Warmuth, A., & Mann, G. 2016, A&A, 588, A115
Woods, T. N., Eparvier, F. G., Hock, R., et al. 2012, SoPh, 275, 115